International Journal of Microwave and Wireless Technologies, 2012, 4(4), 407–412. © Cambridge University Press and the European Microwave Association, 2012
doi:10.1017/S1759078711001152

INDUSTRIAL AND ENGINEERING PAPER

Slot coupled patch antenna in MCM-D for millimeter wave detector matrix applications

VAHID TAVAKOL[1], FENG QI[1], ILJA OCKET[1], DOMINIQUE SCHREURS[1], WALTER DE RAEDT[2] AND BART NAUWELAERS[1]

In this work we assess the feasibility of fabricating a matrix of antennas for the millimeter (mm)-wave band using the "Multi Chip Module – Deposited (MCM-D)" process. The main focus of the design is to minimize the cross coupling between the antennas fabricated on the common substrate. We investigate the use of a virtual cavity formed by metalized vias in order to reduce the cross coupling to the neighboring cells. The radiation efficiency is analyzed in detail, and experimental results of a 2 × 2 array are presented.

Keywords: Millimeter wave antennas, Antenna arrays, Microstrip antennas, Coplanar waveguide (CPW fed).

Received 17 August 2011; Revised 9 December 2011; first published online 30 January 2012

I. INTRODUCTION

Recently, a significant amount of work has been published on millimeter (mm)-wave imaging systems. Although many older systems use a row of detectors, mechanically scanned, to capture the field in a 2D aperture [1], future systems are more likely to use a full 2D detector matrix to form the image [2, 3]. In this paper we investigate the use of a coplanar waveguide (CPW) fed slot coupled patch antenna fabricated using the low-cost thin film MCM-D process [4] for an mm-wave detector matrix. The MCM-D process used in the fabrication of antennas allows relatively easy integration of these antennas with passive and active elements, using the known flip-chip process. A previous work on MCM-D shows the possibility of using this technology in the mm-wave band [5]. Using a high resistive silicon bulk, MCM-D allows fabrication of antennas with less concern about the losses. However when it comes to an array or a matrix of antennas, the main drawback of using a common silicon bulk as the antenna substrate would be the relatively high leakage to neighboring cells. To overcome this problem we have investigated an approach to create a virtual cavity below the antenna using metalized vias inside the bulk.

The paper starts with a description on MCM-D antenna fabrication in Section II. Next, in Section III, we analyze the radiation efficiency in detail. Experimental results are discussed in Section IV and conclusions are drawn in Section V.

[1]Katholieke Universiteit Leuven, Kasteelpark Arenberg 10 bus 2444, B-3001 Leuven, Belgium. Phone: +32 484885390; Fax: +32 16 321986.
[2]Imec Belgium Kapeldreef 75, B-3001 Heverlee, Belgium.
Corresponding author:
V. Tavakol
Email: vahid.tavakol@esat.kuleuven.be

II. ANTENNA DESIGN

As the design of the mm-wave antenna array is strongly influenced by the way it is implemented in the MCM-D process, we will first elaborate on the construction, before detailing the electromagnetic design process.

A) Technology and implementation

The MCM-D stacking consists of a highly resistive silicon bulk ($\varepsilon r = 11.9$, $\rho > 9$ kΩ cm, thickness = 100 μm) and three metal layers isolated with two benzo-cyclobuten (BCB) layers ($\varepsilon r = 2.65$, thickness = 4.5 μm). The top metal layer is a stack of Ti/Cu/Ni/Au ($\sigma = 4.2\text{E} + 7$ S/m, thickness = 5 μm), the second metal is a Ti/Cu/Ti layer ($\sigma = 5.8\text{E} + 7$ S/m, thickness = 3 μm), and the bottom metal is aluminum ($\sigma = 3.7\text{E} + 7$ S/m, thickness = 1 μm). One limitation of this MCM-D process is the rather low accuracy of the BCB thickness. Therefore the antenna has to be designed for an extended bandwidth to compensate for the possible center frequency shift caused by the fabrication. The possibility of introducing solder balls in this technology makes it an attractive choice for flip-chip integration [6].

In terms of antenna implementation, the choice of technology limits us to a patch antenna. Concerning the spacing between the elements, 0.5λ is commonly used to sample the field in the imaging aperture, i.e. in [1].

As seen in Fig. 1(a), the patch antenna is constructed on the top metal layer, and stands on a BCB layer on top of the second metal layer. The second metal layer has been etched in the area below the patch so the two BCB layers, above and below it, can be united constructing a thicker substrate for the antenna. This simply allows a wider bandwidth. However in this topology by omitting the second metal layer, one is left with only one metal layer to construct the feed and the slot. A common solution to this limitation is to

https://doi.org/10.1017/S1759078711001152 Published online by Cambridge University Press

fabricate a CPW fed slot on the lower metal layer (see Fig. 1(a)).

The CPW feed facilitates the measurement process to be performed using Ground-Signal-Ground (GSG) probes on a probe station connected to a network analyzer. One critical point in the antenna design process is the transition from the GSG pad located on the top metal layer to the CPW line in the lower metal layer. This transition has been modeled and simulated separately to allow an optimum performance, see Fig. 1(b). A GSG configuration simplifies the integration of the antenna with other active and passive elements using the flip-chip process [6].

B) Design considerations of the 2 × 2 array

To reduce the surface wave leakage through the BCB layers, we have introduced slot rings around the patch substrate on the metal layers. However, the fact that the feed slot directly sits on the bulk will lead to wave leakage into the common bulk where shielding is relatively difficult. To study the effect of wave leakage inside the silicon bulk two different antennas are designed, one with no shielding inside the bulk and another with metalized vias inside the silicon bulk. The metalized vias form a virtual cavity that confines the fields and leads to lower cross coupling, see Fig. 2.

The slot matching is achieved by tuning the dimensions of a dog bone slot. Other matching techniques, i.e. using an extra section of a transmission line, are also possible [7]. Furthermore, the CPW line has been modified in the area below the patch. This is to compensate for the change of the line impedance where the line reaches the area under the patch. The second metal layer that is partially removed in the area around the patch is also etched on the area above the CPW feed. Entire removal of this layer is not possible and will violate the metal density rules, i.e. there is a limit to the minimum amount of metal coverage on each metal layer. An image of the fabricated 2 × 2 matrix is shown in Fig. 3.

In terms of electromagnetic design, the HFSS full-wave solver has been used to simulate the antenna. In order to model the infinite/large substrate effect, perfect matching layer boundaries are applied to borders of the bulk and the patch substrate (e.g. the BCB layers). Therefore the simulation conditions resemble a single antenna on an infinite bulk. During the design process a single patch antenna has been simulated, but a final verification was performed on a 2 × 2 structure.

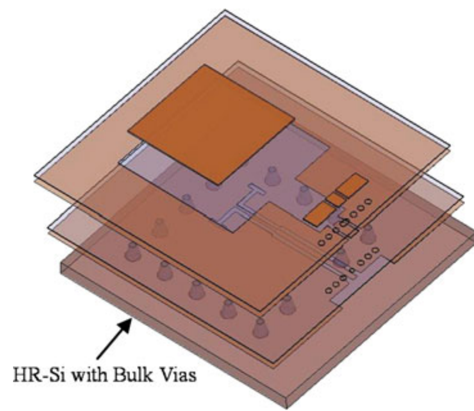

Fig. 2. The patch antenna including silicon bulk vias.

III. RADIATION EFFICIENCY

The radiation efficiency of antennas in thin film processes is usually a critical issue [8]. This is mainly caused by the high intensity of the electrical field in the thin dielectric substrate, which in turn contributes to a high surface current in the rather thin metal layers and eventually an increase in conductor losses.

By definition the radiation efficiency is the power radiated to the power accepted at the input port. One can rewrite the radiation efficiency formula as [5]:

$$\eta = \frac{P_r}{P_r + P_C + P_D + P_{SUR}}, \tag{1}$$

P_r is the radiated power where P_C and P_D are the conductor and dielectric losses, respectively. P_{SUR} is the power dissipated in surface waves traveling along the substrates. We now assess the relative contributions of the various losses to the radiation efficiency by evaluating them with realistic values based on our design case. To keep the calculations reasonable, we consider a single antenna on an infinite bulk substrate.

P_C and P_D are expressed with the formulas below [5]:

$$P_C = 2\sqrt{\frac{\pi f}{\mu_0 \sigma_c}}\frac{W_T}{h}, \tag{2}$$

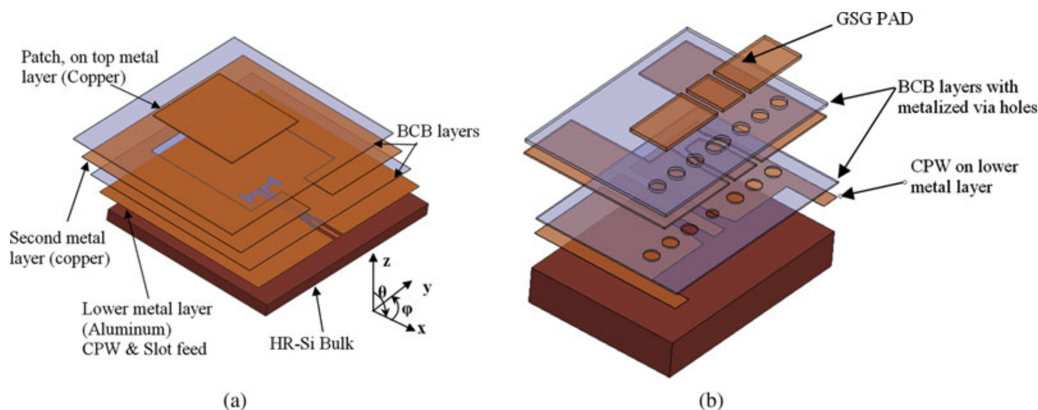

Fig. 1. (a) The patch stacking, by which the second metal layer has been removed around the antenna and CPW feed to allow the combination of the two BCB layers into a single thick substrate for the patch. (b) The feed structure from the top metal layer to the lower CPW line on the first metal layer.

https://doi.org/10.1017/S1759078711001152 Published online by Cambridge University Press

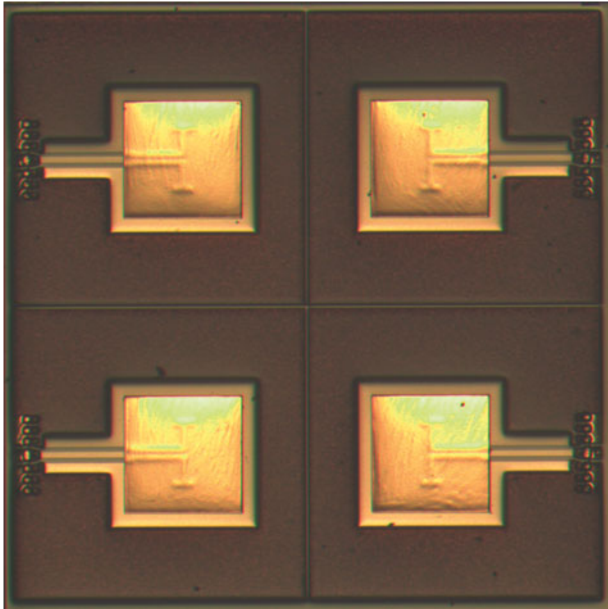

Fig. 3. A microscopic photo of the fabricated 2 × 2 array antenna (cell size is 1.8 × 1.8 mm).

$$P_D = \omega \tan \delta W_T, \quad (3)$$

where W_T is the energy stored in the antenna at resonance, h stands for the substrate height, f for the frequency, and ω for the angular frequency. Moreover tan δ, stands for the dielectric losses, whereas σ_c is the metal (copper) conductivity.

By substituting realistic values, relevant to our design (tan $\delta = 5e-4$, $h = 12$ μm), we arrive at $P_C \approx 35 P_D$. The high conductor losses can be explained by the patch's relatively thin dielectric substrate. By looking at (2) we observe that conductor losses increase with a decrease in dielectric thickness. Even with the combination of the two available layers, as described in Section II, the thickness would not exceed 12 μm.

Furthermore, we can see that both losses increase proportional to the maximum energy stored in the antenna which on its turn is directly related to the dielectric constant [9].

Since the dog bone slot sits directly on the silicon bulk, two elements will contribute to the P_{SUR}. First we have the surface waves excited in the patch's BCB substrate, P_{SUR_BCB}, and secondly we have the surface waves traveling inside the silicon, P_{SUR_SI}:

$$P_{SUR} = P_{SUR_BCB} + P_{SUR_SI}. \quad (4)$$

According to the study in [10], as long as the thickness satisfies,

$$\frac{h}{\lambda_0} \leq \frac{0.3}{2\pi\sqrt{\varepsilon_r}}, \quad (5)$$

the surface wave losses will be negligible in comparison to the conductor and dielectric losses. For our case this is true for the P_{SUR_BCB} term in (4), while it does not stand for the P_{SUR_SI} term, as the bulk thickness is 100 μm. Here we observe another advantage of bulk vias, namely in blocking the propagation of surface waves and therefore possibly contributing to improved radiation efficiency. The radiation efficiency calculated using HFSS is roughly 18% for the antennas on a normal bulk, whereas this value shows an increase, to 25%, for the antennas created over a virtual cavity. To calculate the total power carried away by surface waves inside the substrate (*e.g.* P_{SUR_SI}), we can evaluate the Poynting vector integral on the edge boundaries of the substrate. This calculation reveals that, P_{SUR_SI} decreases from 0.44 to 0.26 W by introducing the virtual cavity. The Poynting vector calculations are done for 1 W incident power at 100 GHz. Although this reduction is considerable, it does not contribute as much to an increase in efficiency. This can be explained by the increased conductor losses caused by higher electrical field intensities. To validate this we have integrated the conductor losses over the surface of Metal 1, i.e. the lowest metal layer that sits directly above the cavity. By adding the cavity, conductor losses on this metal layer showed an increase from 0.08 to 0.21 W.

IV. RESULTS

A number of 2 × 2 arrays have been fabricated. Below we present a summary of the return loss and isolation measurements followed by the radiation pattern simulations.

A) Return loss and isolation

To measure the return loss and insertion loss of two front facing antennas, a probe station connected to a vector network analyzer is used. The return loss, S_{11}, of both designs, i.e. with and without bulk vias, is measured and compared with the simulated results in Fig. 4. Apart from the frequency shift of the measured results, there is also a slight shift (from 100 GHz target design center) present in the simulations results. This is simply because of the fact that the simulated results presented here are from the 2 × 2 array antenna, whereas during the design process a single antenna on an infinite bulk has been optimized to operate at 100 GHz. The main reason for this is the huge meshing requirement of the 2 × 2 array calculations that would not allow simulations to complete in a reasonable time.

The measured return loss shows a slight shift compared to the original design. As explained in Section II, the detuning of the patch center frequency was expected to be present and is attributed to the limited accuracy of the BCB thickness. In this specific process run, the thickness of the second BCB layer varies from a minimum of 7.5 μm to a maximum of 9.5 μm, with a target of 8.5 μm. We also observe that there is no difference in terms of return loss between the antenna array with and without bulk vias. The reported −7 dB bandwidths for microstrip fed rectangular patches in MCM-D [5] are 2.9 and 3.7% at 82 and 79 GHz, respectively, whereas the bandwidth achieved in this study (−10 dB, centered at 98 GHz) is 6.1% for antennas on normal bulk and 7.8% for antennas with bulk vias.

The measured and simulated cross coupling, S_{21}, is presented in Fig. 5. The isolation presented here is for the worse case (front facing antennas) where the radiation edges of the two patches are parallel to each other. As clearly seen

https://doi.org/10.1017/S1759078711001152 Published online by Cambridge University Press

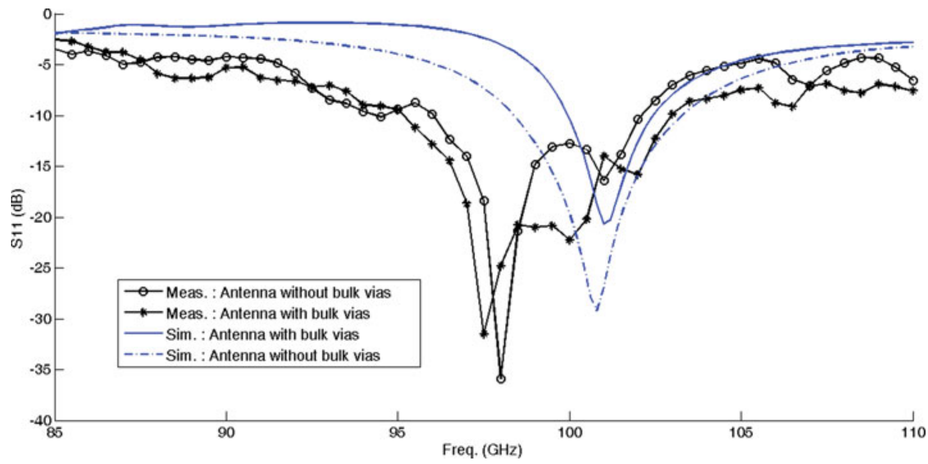

Fig. 4. Comparison of measured and simulated return loss of the 2 × 2 antenna array with and without bulk vias.

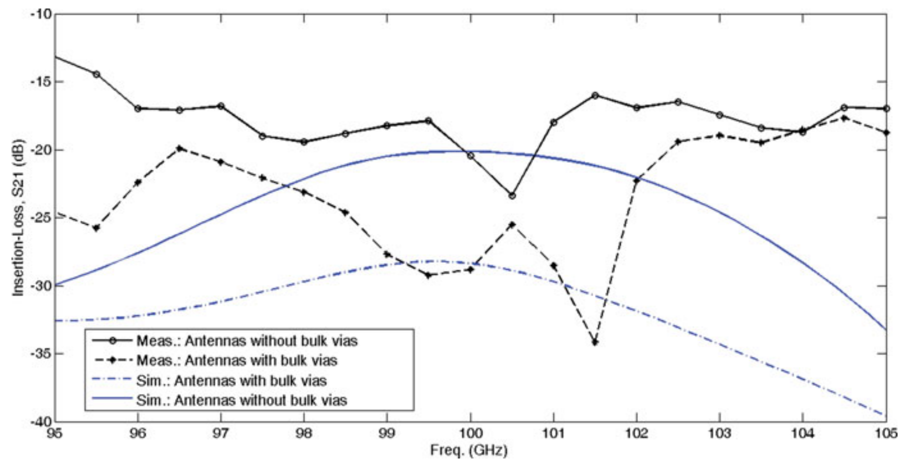

Fig. 5. Comparison of measured and simulated isolation between two front facing antennas both with and without bulk vias.

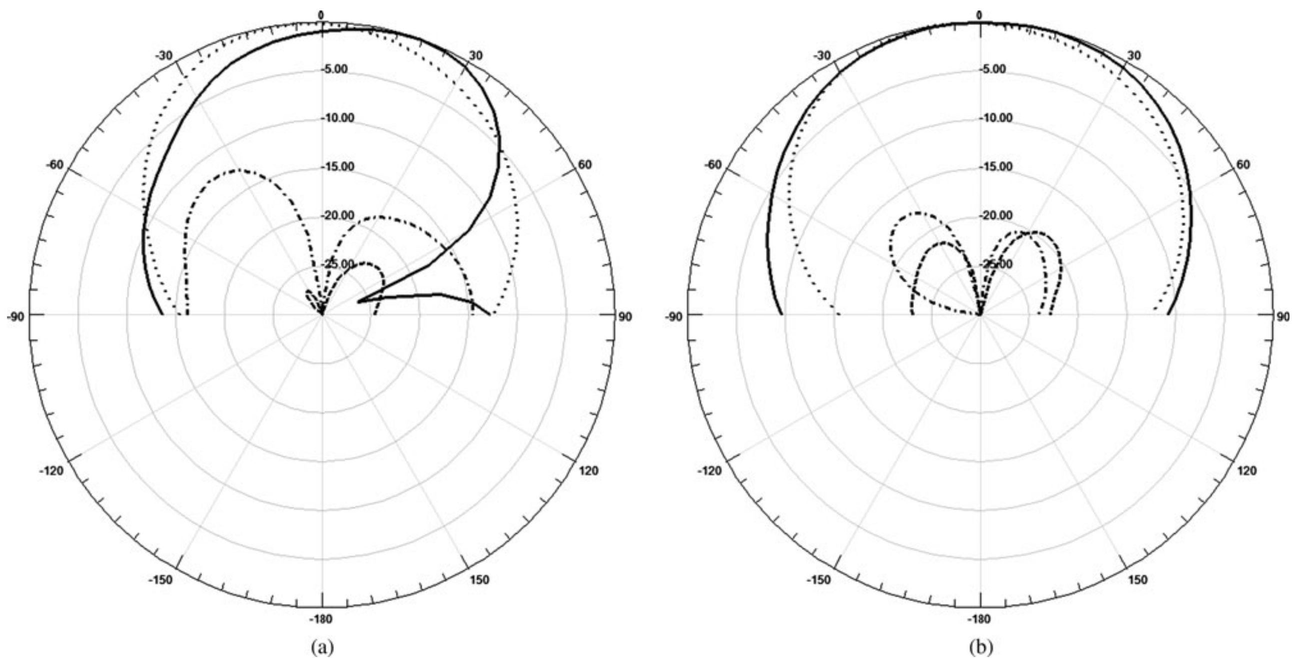

Fig. 6. Simulated radiation patterns of a single element in a 4 × 4 array (normalized to maximum value) in E-plane (phi = 0) and in H-plane (phi = 90) (referring to axis definitions in Fig. 1): (a) for the antenna without bulk vias and (b) for the antenna with bulk vias.

https://doi.org/10.1017/S1759078711001152 Published online by Cambridge University Press

on Fig. 5 the antennas with shielding vias inside the substrate show an average of 10 dB improved isolation performance.

B) Radiation patterns

Radiation pattern measurement at 100 GHz, with a reasonable accuracy, is extremely challenging and scarcely available. Knowing that the accuracy of the solver has been verified by return loss measurements, it would not be unreasonable to rely on the simulated results for the radiation patterns. The normalized radiation patterns of both antennas are presented in Fig. 6. The co-polar element, E-theta in phi = 0°, and E-phi in phi = 90°, are plotted for both antennas (for the axis definitions refer to Fig. 1). The simulated results are for a single antenna inside a 2×2 array on an infinite bulk, i.e. only one antenna port is excited and the other ports are terminated by 50 Ω. By introducing substrate vias we intend to reduce the cross coupling and loading of adjacent cells, while also to improve the pattern performance caused by presence of neighboring antennas. As clearly seen in Fig. 6 the radiation pattern of the antenna with substrate vias shows no nulls in E-plane while the other one has a null at 75°. The presence of this null can be attributed to the current excitation on the edge of the front facing antenna. By confining the bulk fields inside the virtual cavity, we can avoid the excitation of the front facing antenna. By using the substrate vias we managed to achieve a uniform radiation pattern similar to a single patch antenna (see Fig. 6(b)).

As these antennas are aimed for an mm-wave imaging system, we focused on a single linear polarized element. Clearly seen in Fig. 6(b), the cross-polar component is well below the co-polar one indicating a linearly polarized antenna.

Here another advantage of the virtual cavity becomes evident. Namely the reader must keep in mind that this is a matrix of antennas rather than an array, and therefore the performance of each single element is of interest.

V. CONCLUSIONS

The MCM-D process has been studied to fabricate patch antennas operating at 100 GHz for mm-wave detector matrix applications. Combining the two dielectric layers available in this technology, we have managed to gain an acceptable performance both in terms of bandwidth and efficiency. Using silicon bulk vias, we have managed to reduce the cross coupling between different elements. We also managed to obtain an improved radiation pattern. This increases the applicability of this technology for matrix applications where reducing the interference between neighboring cells is of critical importance. A study on the efficiency shows that the dominant reduction is caused by the thin patch substrate contributing to high metal losses. We would suggest other variations of MCM-D (*e.g.* similar to [11]) with thicker BCB layers for future investigations.

REFERENCES

[1] Sheen, D.M.; McMakin, D.L.; Hall, T.E.: Three-dimensional millimeter-wave imaging for concealed weapon detection. IEEE Trans. Microw. Theory Tech., **49** (2001), 1581–1592.

[2] Lovberg, J.A.; Martin, C.; Kolinko, Y.: Video-rate passive millimeter-wave imaging using phased arrays. In Proc. of IEEE/MTT-S Int. Microwave Symp., Honolulu, HI, June 2007, pp. 1689–1692.

[3] Ahmed, S.S.; Schiess, A.; Schmidt, L.P.: Near field mm-wave imaging with multistatic sparse 2D-arrays. In European Radar Conf., EuRAD 2009, Rome, Italy, September 30–October 2, 2009, pp. 180–183.

[4] Posada, H.; Carchon, G.; Nauwelaers, B.; De Raedt, W.: Thin-film MCM-D technology with through-substrate vias for the integration of 3D SiP modules. In Proc. of Electronic Components and Technology Conf., Lake Buena Vista, FL, May 2008, pp. 2060–2066.

[5] Grzyb, J.; Troster, G.: mm-wave microstrip and novel slot antennas on low cost large area panel MCM-D substrates – a feasibility and performance study. IEEE Trans. Adv. Packag., **25** (3) (2002), 397–408.

[6] Perfecto, E.D.; Shields, R.R.; Master, R.N.: A low cost MCM-D process for flip chip and wirebonding applications. In Electronic Components and Technology Conf., May 1995, pp. 1081–1086.

[7] Hettak, K.; Delisle, G.; Boulmalf, M.: A novel integrated antenna for millimeter-wave personal communications systems. IEEE Trans. Antennas Propag., **AP-46** (1998), 1757–1758.

[8] Verma, A.; Fumeaux, C.; Van-Tan, T.; Bates, B.D.: Effect of film thickness on the radiation efficiency of a 4.5 GHz polypyrrole conducting polymer patch antenna. In Microwave Conf. Proc. (APMC), 2010, Yokohama, Japan, December 7–10, 2010, pp. 95–98.

[9] Sheen, J.: Losses of the parallel-plate dielectric resonator. IET Microw. Antennas Propag., **2** (3) (2008), 221–228.

[10] James, J.R.; Henderson, A.: High-frequency behaviour of microstrip open-circuit terminations. IEE J. Microw. Opt. Acoust., **3** (1979), 205–218.

[11] Platt, D.; Pettersson, L.; Jakonis, D.; Salter, M.; Hagglund, J.: Integrated 79 GHz UWB automotive radar front-end based on hi-mission MCM-D silicon platform. In European Radar Conf., EuRAD 2009, Rome, Italy, September 30–October 2, 2009, pp. 445–448.

Vahid Tavakol received his B.Sc. in electrical engineering from University of Tehran, Iran in 2003. He graduated with an M.Sc. in hardware for wireless technology from Chalmers University of Technology, Goteborg, Sweden in 2006. He is currently working toward the Ph.D. in Catholic University of Leuven, Belgium. His main research interests include mm-wave antennas and mm-wave frontends.

Feng Qi received his Ph.D. degree in electrical engineering from Catholic University of Leuven. He joined RIKEN as a Foreign Postdoctoral Researcher in June 2011. He is currently working on ultra-wide band, monochromatic THz generation and detection systems, aiming at novel applications. His research interests include mmW/THz imaging and sensing, synthetic aperture radar, antennas and antenna array design, nonlinear optics, and interaction between waves and matters.

https://doi.org/10.1017/S1759078711001152 Published online by Cambridge University Press

Ilja Ocket received his M.Sc. and Ph.D. degrees in electrical engineering from the Catholic University of Leuven in 1998 and 2009. His interests include all aspects of millimeter-wave and microwave applications and systems, with a particular interest in antennas and advanced packaging technologies for heterogeneous systems. In the past he has worked on projects involving automotive radar at 77 GHz, wireless communications at 60 GHz and millimeter-wave imaging. He currently works on the development of millimeter-wave biomedical and identification systems.

Dominique M. M.-P. Schreurs received the M.Sc. and Ph.D. degrees in electronic engineering from the Katholieke Universiteit (K.U.)Leuven, Belgium. She is now Associate Professor at K.U.Leuven. She has been Visiting Scientist with ETH Zürich (Switzerland), NIST, and Agilent (USA). Her main research interests concern the (non)linear characterization and modeling of active microwave devices and circuits, as well as (non)linear hybrid and integrated circuit design for telecommunications and biomedical applications. D. Schreurs serves on the IEEE MTT-S Administrative Committee. She has been appointed as Distinguished Microwave Lecturer for the term 2012–2014. D. Schreurs also serves on the ARFTG Executive Committee and is General Chair of the 2012 ARFTG Spring Conference. D. Schreurs is Associate Editor for IEEE Microwave and Wireless Components Letters and for the International Journal of Microwave and Wireless Technologies.

Walter De Raedt graduated in electrical engineering (1981) at K.U.Leuven, Belgium. From 1981 to 1984 his research focused on e-beam technology at K.U.Leuven labs. In 1984 he joined IMEC at its start as a project leader in charge of submicron technologies for advanced HEMT devices until 1997. In 1987 he was visiting scientist at IBM Rüschlikon working on fast III–V circuits. From 1997, he joined the MCM group at IMEC in charge of the design, modeling, and characterization activities for packaging. Currently, he is head of the RFCDM group at IMEC and was involved in many EU research projects (MIPA, 3DμTune, Shift, e-cubes, etc.). In 2003 he received the IEEE microwave prize with his team. He authored and co-authored more than 200 papers, several patents, and book chapters in the field of microwave/mm-wave modeling, design, and packaging. His current interests are in the field of MEMS-based solutions and SiP (System in package) integration for wireless systems.

Bart. K. J. C. Nauwelaers received the M.S. and Ph.D. degrees in electrical engineering from the K.U.Leuven, Belgium in 1981 and 1988, respectively. He also holds a Mastère degree in design of telecommunication systems from ParisTech Télécom, France. He is a full professor at K.U.Leuven, where he teaches in the fields of microwaves and digital communications. His research interest are in MMICs, linear and non-linear device modeling, MEMS, and interconnect technologies.

https://doi.org/10.1017/S1759078711001152 Published online by Cambridge University Press